On-Chip Strong Coupling and Efficient Frequency Conversion between Telecom and Visible Optical Modes

Xiang Guo, Chang-Ling Zou, Hojoong Jung, and Hong X. Tang

Phys. Rev. Lett. **117**, 123902 — Published 16 September 2016

DOI: 10.1103/PhysRevLett.117.123902

On-chip strong coupling and efficient frequency conversion between telecom and visible optical modes

Xiang Guo,[1] Chang-Ling Zou,[1] Hojoong Jung,[1] and Hong X. Tang*[1]

[1]*Department of Electrical Engineering, Yale University, New Haven, Connecticut 06511, USA*

While frequency conversion of photons has been realized with various approaches, the realization of strong coupling between optical modes of different colors has never been reported. Here, we present an experimental demonstration of strong coupling between telecom (1550 nm) and visible (775 nm) optical modes on an aluminum nitride photonic chip. The non-reciprocal normal-mode splitting is demonstrated as a result of the coherent interference between photons with different colors. Furthermore, a wide-band, bi-directional frequency conversion with 0.14 on-chip conversion efficiency and a bandwidth up to 1.2 GHz is demonstrated.

Developments in classical and quantum information technologies have spurred the study of photonics, attributing to photon's long decoherence time, low transmission loss and high speed. Coherent coupling between photons with various matter qubit systems such as atomic ensembles [1] and quantum dots [2] is realized. These systems, however, favor photons of visible or near infrared wavelength, which are not suitable for long distance communication through fiber. As a result, coherent frequency conversion between visible and telecom bands is of great interests and has been realized with different methods, including three wave mixing ($\chi^{(2)}$ nonlinearity) [3–6], four wave mixing ($\chi^{(3)}$ nonlinearity) [7–9] and opto-mechanical interactions [10, 11]. Among them, the implementations of frequency conversion with integrated photonic devices [12, 13] are of special interests due to device's small foot-prints and scalability [14, 15]. In addition, owing to the high quality factor to mode volume ratio, micro-cavity based devices are promising for enhanced photon-photon interactions.

In this Letter, we demonstrate the strong coupling between optical modes of different colors on a scalable aluminum nitride-on-insulator [16] chip, bringing the cavity nonlinear optics into a new regime, and also offering a unique way to realize all-optical control, isolation and efficient frequency conversion. Under the parametric pumping of an optical drive field, normal-mode splitting [1, 17] is observed, which is the benchmark for coherent coupling between the visible mode and the telecom mode. Due to the inherent phase matching condition in the traveling wave cavity, the demonstrated coherent interaction and the accompanying mode splitting are non-reciprocal [18, 19], which permits future applications such as non-magnetic, ultrafast optical isolators [20–22]. We further realize bi-directional optical frequency conversion between telecom band and visible band with 0.14 on-chip (photon flux) conversion efficiency. The demonstrated strong coupling between photons of different colors is of fundamental interest for quantum optics and provides a kernel device for the realization of quantum internet [23].

Figure 1(a) illustrates the fabricated aluminum nitride (AlN) microring structure. The $\chi^{(2)}$ nonlinearity of the AlN microring induces the interaction between three modes of different colors. We choose transverse-magnetic (TM) modes because TM mode has higher $\chi^{(2)}$ nonlinearity as compared to transverse-electric (TE) modes in our AlN

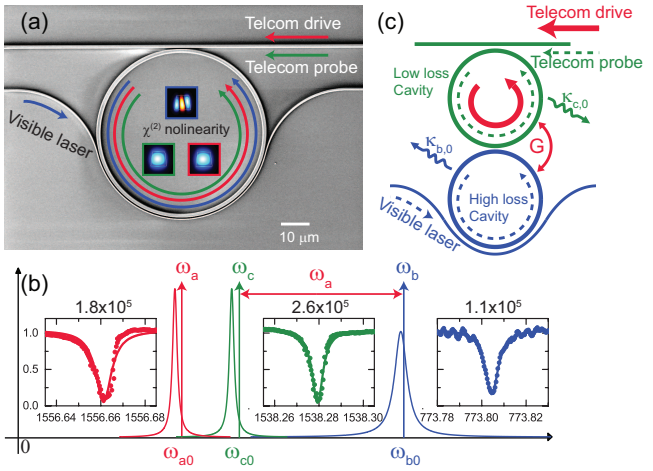

FIG. 1: Triply resonant microring resonator coupled by second order optical nonlinearity. (a) SEM picture of the core device. Three optical modes co-exist in the microring resonator, and couple through $\chi^{(2)}$ nonlinear interaction. Insets are the field distributions of the cross-section. (b) Schematics of the optical modes' frequencies and their respective transmission spectrum. (c) Coupled resonator model for the coherent interaction in a $\chi^{(2)}$ microring resonator. Here the coupling between telecom and visible probe modes is controlled by the telecom drive laser.

chip. To fulfill the required phase match condition of three-wave mixing process, we engineer the width of the microring [24, 25] to match the refractive index of the fundamental TM (TM_0) mode in telecom band to the refractive index of third order TM (TM_2) mode in visible band. Their respective mode profiles are shown in the insets of Fig. 1(a). Because dual wavelength bands are involved in this system, we design two bus waveguides to couple with telecom TM_0 mode and visible TM_2 mode separately (Fig. 1(a)). In the following we adopt an quantum optics description of our system, although a classical description is also viable. The three wave mixing in the microring can be described by the Hamiltonian

$$\mathcal{H} = \omega_{a0}\hat{a}^\dagger\hat{a} + \omega_{b0}\hat{b}^\dagger\hat{b} + \omega_{c0}\hat{c}^\dagger\hat{c} + g(\hat{a}\hat{b}^\dagger\hat{c} + \hat{a}^\dagger\hat{b}\hat{c}^\dagger). \quad (1)$$

Here, $\hat{a}$, $\hat{b}$ and $\hat{c}$ are the Bosonic operators for three TM modes in the microring. g is the nonlinear single-photon interaction strength and is dependent on $\chi^{(2)}$ coefficient of the material, field overlap for three modes as well as

mode volumes [26]. Additionally, the momentum conservation condition ($m_a + m_c = m_b$) must be fulfilled for a non-vanishing g, which demands all three modes traveling in the same direction in the microring resonator to get involved in the nonlinear interaction process. This directivity further results in a non-reciprocal transmission spectrum for the probe mode's resonance. In the experiment, we choose modes a, c in the telecom band and mode b in the visible band. The measured transmission spectra of the modes and the schematic diagram of their frequencies are depicted in Fig. 1(b). Here, telecom modes a and c are almost critically coupled [30] ($\kappa_{a,1}(\kappa_{c,1}) = \kappa_{a,0}(\kappa_{c,0})$, where $\kappa_{x,0}(\kappa_{x,1})$ is the intrinsic (external) loss rate of mode x), while visible mode b is slightly under-coupled ($\kappa_{b,1} < \kappa_{b,0}$). The loaded quality factors and linewidth for modes a, b and c are $Q_{load,a}(Q_{load,b}, Q_{load,c}) = 1.8\times10^5(1.1\times10^5, 2.6\times10^5)$ and 1.08 GHz(3.53 GHz, 0.74 GHz), respectively.

As we aim for the coherent coupling between the telecom and visible photons, we strongly drive mode a by a near resonance strong laser (ω_a) and hence stimulate large exchange coupling strength between mode b and c. The simplified system Hamiltonian reads [26]

$$\mathcal{H} = \omega_{b0}\hat{b}^\dagger\hat{b} + \omega_{c0}\hat{c}^\dagger\hat{c} + G\hat{c}\hat{b}^\dagger e^{-i\omega_a t} + G^*\hat{c}^\dagger\hat{b}e^{i\omega_a t}, \qquad (2)$$

where $G = \langle\hat{a}\rangle\, g$ is the effective interaction strength, with $|\langle\hat{a}\rangle|^2 \propto P_a$ is the mean photon number of mode a and P_a is the power of the drive laser. This beamsplitter-like Hamiltonian indicates that photons in cavities b and c can be converted to each other coherently without introducing additional noises [3], just like a linear optics device.

It is instructive to introduce a simplified model, as depicted in Fig. 1(c), where two resonators loaded by two separate bus waveguides are used to represent the resonant modes b and c separately. We model the effective interaction strength G as a controllable coupling switch between the two optical modes with different colors. If there is no driving ($G = 0$), the two resonators are decoupled from each other and photons cannot tunnel from one ring to the other (physically, this means photons cannot change color without nonlinear interaction). When the drive laser is on and nonlinear interaction G is nonzero, the two ring cavities start to couple together and photons in one resonator can couple into the other one (physically, it means that photons' colors get changed due to nonlinear interaction) and even coupled back when the G is comparable to the cavities' loss rates. Note that this nonlinear interaction process is non-reciprocal because G vanishes for the probe lights propagating in the opposite direction of the drive laser due to momentum mismatch [26].

From the schematic illustrated by Fig. 1(c), the most straightforward outcome of the coherent coupling between two coupled resonators is the modified resonance spectrum. We can also see this via the energy diagram [26], where two pathways are connected to the same energy level and induce interference [31]. Physically, when visible photons enter the microring, they can be coherently scattered into telecom photons by the strong drive laser. The generated telecom photons can be converted back to visible photons and result in destructive interference for the probe laser. When the coupling strength G is comparable or even larger than the resonators' dissipation rates, the coherent conversion beats the decoherence and normal-mode splitting emerges. Using the experimental setup shown in Fig. 2(a), the transmission spectrum of visible mode is probed. The telecom drive laser (ω_a, near the resonant frequency ω_{a0} of mode a) excites the counter-clockwise (CCW) propagating mode in the microring, while a visible laser (ω_b) probes the transmission of mode b (centered at ω_{b0}) in either clockwise (CW) or CCW direction. Figure 2(b) plots the spectra of mode b probed from different directions with drive laser fixed. A mode splitting spectrum is observed when the visible laser propagates in the same direction (CCW) as the drive laser. In contrast, when the probe laser propagates in the counter-propagating direction (CW) of the drive laser, the resonance is of normal Lorentzian shape, similar to the transmission spectrum without parametric pumping (Fig. 2(c), top panel). The comparison of the spectra for two propagating directions clearly reveals the non-reciprocal nonlinear effect in the microring.

The observed mode splitting is further tested with different powers of the drive laser (Fig. 2(c)). A clearly increased splitting level is observed with the increase of launched drive laser power. Following the Hamiltonian (Eq. (2)) and considering the linear losses of modes b and c, we derive the theoretical formula for the transmission of the visible mode b as

$$T = \left|1 + \frac{2\kappa_{b,1}}{-i\delta_b - \kappa_b + \frac{|G|^2}{-i\delta_c - \kappa_c}}\right|^2, \qquad (3)$$

where $\kappa_{a(b)} = \kappa_{a(b),0} + \kappa_{a(b),1}$ is total loss rate, $\delta_b = \omega_{b0} - \omega_b$ and $\delta_c = \omega_{c0} - (\omega_b - \omega_a)$ are the angular frequency detunings of mode b and c, respectively. The experimental results are fitted according to Eq. (3) and exhibit valid agreements, as shown by the red solid lines in Fig. 2(c). Here $\kappa_{b(c)}$, $\kappa_{b,1}$, G and $\Delta = \delta_c - \delta_b = \omega_a + \omega_{c0} - \omega_{b0}$ are treated as fitting parameters. Cooperativity $C = \frac{|G|^2}{\kappa_b\kappa_c}$ [10, 11, 19, 31] is usually used in hybrid systems as a figure-of-merit to evaluate the coherent coupling between two different modes. It is closely related to the concept of strong coupling, where the coupling strength is bigger than the loss rates of both modes ($|G| > \kappa_b, \kappa_c$). To quantify the coherent interaction strength, the cooperativity C is extracted from each transmission spectrum and plotted against drive laser power P_a (Fig. 2(d)). The linear dependence of C over the launched drive power is observed, as expected by theory that $C \propto |G|^2 \propto P_a$. From the data in Fig. 2(d), a unit power cooperativity of $C/P_a = 0.042 \pm 0.001\,\mathrm{mW}^{-1}$ is derived. Specifically, with the highest power we applied (83.7 mW), a maximum cooperativity of 3.53 is achieved with $|G| = 2\pi \times 1.38$ GHz, $\kappa_b = 2\pi \times 1.00$ GHz and $\kappa_c = 2\pi \times 0.54$ GHz. The strong coupling ($|G| > \kappa_b, \kappa_c$) is clearly observed from the bottom-most curve in Fig. 2(c), which indicates that the telecom and visible modes are coherently coupled and hybridized into two dressed states, whose frequencies read:

$$\omega_\pm = \omega_{b0} + \frac{1}{2}\Delta \pm \frac{1}{2}\sqrt{4G^2 + \Delta^2} \qquad (4)$$

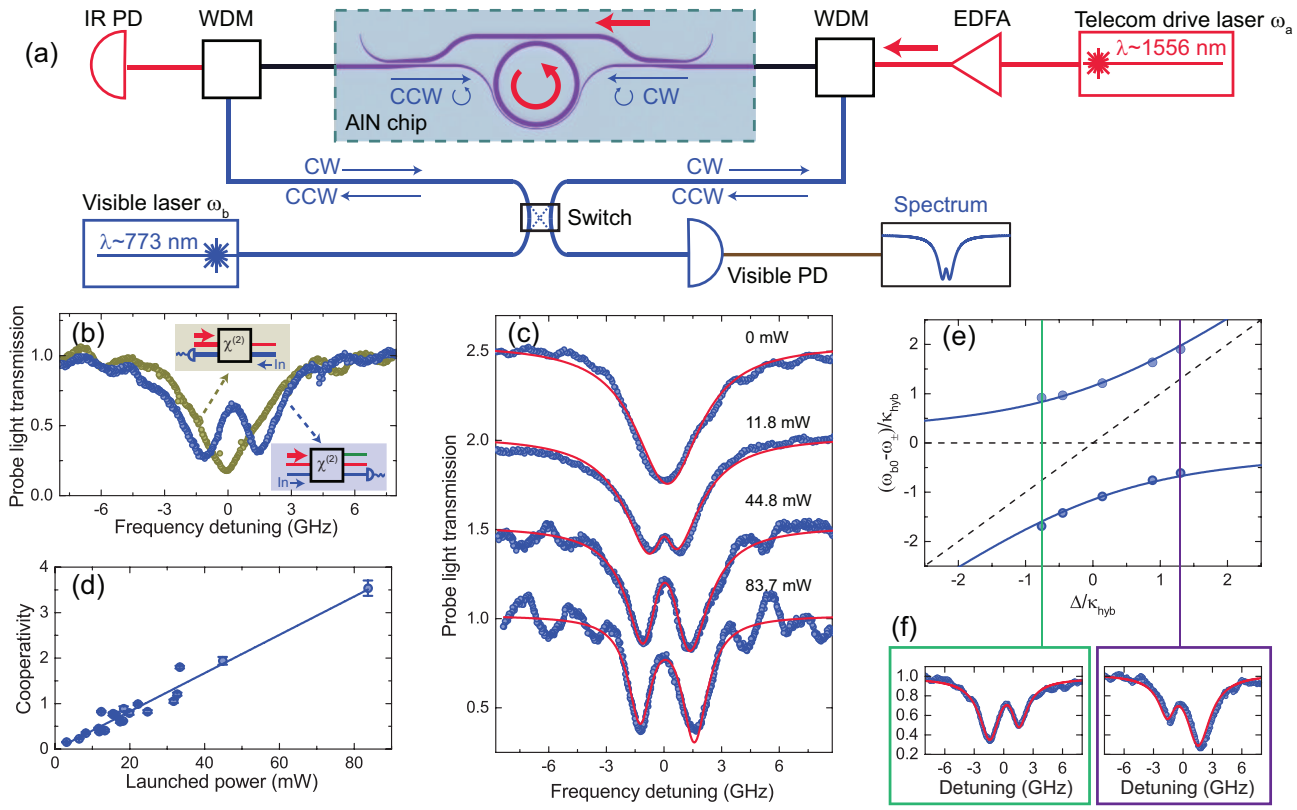

FIG. 2: Strong coupling due to $\chi^{(2)}$ nonlinear interaction. (a) Experimental setup. Telecom laser ω_a strongly excites mode a in the microring resonator with CCW propagation direction. A visible probe laser ω_b is used to probe the transmission spectrum of mode b (centered at ω_{b0}) from either CW or CCW direction. (b) Transmission spectra of mode b with either CW or CCW directions. The data is plotted in linear scale. In both insets, the giant red arrow represents the input direction of the telecom drive laser while the blue arrow represents the input direction of the visible probe laser. (c) Modified visible transmission spectra under different drive powers. The red solid lines are fittings with Eq. (3). The transmission in the center of the resonance increases from 27% (with 0 mW drive power) to 80% (with 83.7 mW drive power) of the total transmission. The data is shown in linear scale, and the vertical axes of the four transmission curves have been offset for clarity. (d) Extracted cooperativities at different drive powers. (e) Frequencies of dressed modes ($\omega_\pm$) under different values of Δ. The solid line is the theoretical fitting curve. (f) Fano-like transmission spectra when $\Delta \neq 0$.

The extracted values of $\omega_\pm$ from experiment data are plotted in Fig. 2(e), where a clear avoid-crossing behavior is observed and agrees well with the fittings. When the detuning $\Delta = 0$, the minimum of the splitting is $2G$ ($\omega_\pm = \omega_{b0} \pm G$) and the spectrum is the sum of two identical Lorentzian shapes with linewidth of $\kappa_{hyb} = (\kappa_b + \kappa_c)/2$. When $\Delta \neq 0$, Fano-like shapes can be observed in the transmission spectrum as shown in Fig. 2(f). Compared with other nonlinearly coupled systems such as opto-mechanical [32] and magneto-optical [33] systems, our system has much higher interaction strength G. The cooperativity of our system, however, is currently lower than the opto-mechanical systems [32] due to higher loss rate (on the order of GHz) of our optical modes compared to the low frequency mechanical mode (whose loss rate is on the order of kHz).

While the normal-mode splitting is the hallmark of the coherent interaction, another manifestation of the large coupling between the telecom and visible modes is the high efficiency frequency conversion. From frequency conversion point of view, the device acts as a beamsplitter for different colors of light and the splitting ratio is controlled by the drive laser. As schematically illustrated in the insets of Fig. 3(b), the on-chip conversion efficiency (ratio of photons flux in the output waveguide to the photon flux in the input waveguide) is measured for both up- and down-conversion. The wavelength conversion spectra under different drive laser powers are shown in Fig. 3(a). It is observed that the spectrum is of Lorentzian shape under relative weak drive power. When the drive laser power is strong enough, the conversion spectrum starts to split. The on-chip conversion efficiency for both up- and down-conversion reads

$$\eta_{oc} = \frac{\kappa_{b,1}}{\kappa_b}\frac{\kappa_{c,1}}{\kappa_c} \times \frac{4C}{\left|(1+i\frac{\delta_b}{\kappa_b})(1+i\frac{\delta_c}{\kappa_c})+C\right|^2}. \quad (5)$$

For near-resonance condition that $\delta_c \approx \delta_b \approx 0$

$$\eta_{oc,max} \approx \frac{\kappa_{b,1}}{\kappa_b}\frac{\kappa_{c,1}}{\kappa_c} \times \frac{4C}{|1+C|^2}. \quad (6)$$

We plot the conversion efficiency against the launched drive laser power as shown in Fig. 3(b). By fitting the experimental results with Eq. (6), we deduce a unit power cooperativity of $0.041 \pm 0.004\,\mathrm{mW}^{-1}$, which agrees well with the value obtained from mode splitting measurement. According to Eq. (6), the maximum on-chip conversion efficiency

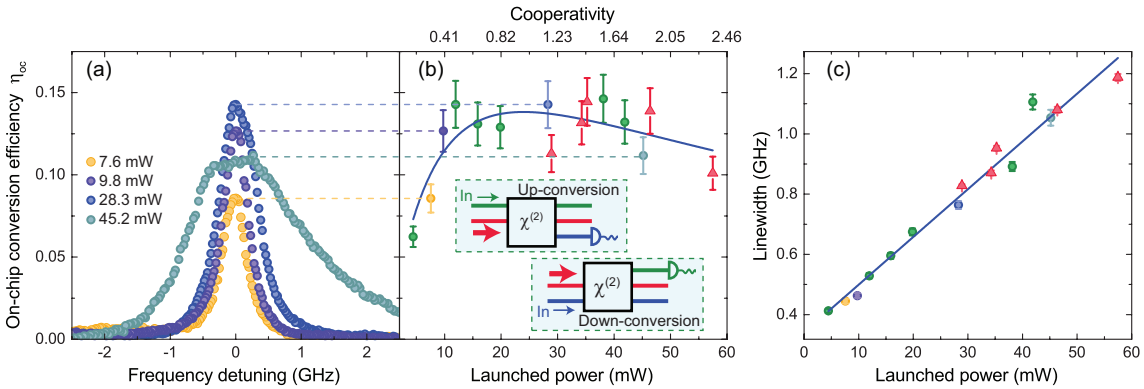

FIG. 3: Optical frequency conversion between the telecom and the visible band. (a) Frequency conversion spectra under different drive laser powers. (b) On-chip conversion efficiency against drive power. The error bar comes from the uncertainty of the fiber-to-chip insertion loss. Triangle data points correspond to frequency down-conversion, while circles correspond to frequency up-conversion. The blue solid line is a fitted curve according to Eq. (6). In both insets, the giant red arrow represents the telecom drive laser. The blue (green) arrow represents seed power of visible (telecom) probe laser. (c) The linewidth of the frequency conversion spectra under different drive powers.

will be achieved when $C \approx 1$, which corresponds to a drive laser power around 24.4 mW. Due to non-ideal waveguide-to-microring coupling ($\frac{\kappa_{c,1}}{\kappa_c} \approx 0.5$, $\frac{\kappa_{b,1}}{\kappa_b} \approx 0.3$), the achievable on-chip conversion efficiency is limited to be around 0.14. To further increase the on-chip conversion efficiency, both telecom and visible modes need to be over-coupled ($\kappa_{c,1} > \kappa_{c,0}$, $\kappa_{b,1} > \kappa_{b,0}$) while the cooperativity remains as 1. We further study the bandwidth of the frequency conversion under different drive power P_a (Fig. 3(c)). The nonlinear conversion bandwidth ($\frac{\kappa_{cov}}{2\pi}$) is dependent on the linewidth of both mode b and c, as well as the cooperativity C. We observe a linearly increased conversion bandwidth with increased cooperativity, matching well with the theory that $\frac{\kappa_{cov}}{2\pi} = \frac{1}{2\pi}\frac{\kappa_b\kappa_c}{\kappa_b+\kappa_c}(1+C)$. A largest bandwidth of 1.2 GHz is achieved with a drive laser power of 57.5 mW. A unit power cooperativity of $0.046 \pm 0.004\,\mathrm{mW}^{-1}$ is fitted from the data in Fig. 3(c), being consistent with the values extracted from Fig. 2(d) and Fig. 3(b).

The unit power cooperativity is related to the nonlinear single-photon interaction strength g and the linewidth of the optical mode

$$\frac{C}{P_a} = \frac{g^2}{\kappa_a\kappa_b\kappa_c \cdot \hbar\omega_a}. \tag{7}$$

By using thick AlN film (1 μm-thick), the waveguide size increases and has better confinement of the optical mode. In addition, we cover the AlN waveguide with SiO_2 top claddings to decrease the refractive index difference and hence the scattering loss. All of these help to reduce the microring radius and increase the quality factors of the optical modes. We also use TM modes to replace TE modes for higher $\chi^{(2)}$ nonlinearity. These changes lead to a four order of magnitude improvements in terms of unit power cooperativity as compared to our previous work [34], making it possible to enter strong coupling regime. The nonlinear single-photon interaction strength g can be estimated as $g = \sqrt{\frac{C}{P_a} \cdot \kappa_a\kappa_b\kappa_c \cdot \hbar\omega_a} \approx 0.74\,\mathrm{MHz}$, which is consistent with the theoretically estimated value by assuming $\chi^{(2)} = 1.3\,\mathrm{pm/V}$ [26].

The cooperativity of the system may be further improved. Firstly, in current experiment the position of the involved optical modes has not been perfectly aligned ($\omega_{a0}+\omega_{c0}-\omega_{b0} \neq 0$). To induce symmetric mode splitting, the drive laser frequency is set to be $\omega_a = \omega_{b0} - \omega_{c0} \neq \omega_{a0}$, which means that the drive laser is detuned from the resonance of mode a and the effective coupling strength G is hence reduced. By placing an on-chip heater in the microring, we can finely tune the position of the optical modes through thermal-optical effect and perfectly fulfill phase match condition ($\omega_{a0}+\omega_{c0} = \omega_{b0}$), leading to higher cooperativity. Secondly, single-photon coupling strength g can be improved by reducing mode volume [26]. Thirdly, the quality factor itself can be improved by using even thicker AlN film. Lastly, by applying high peak power driving pulses, the transient driving photon numbers may be improved. For quantum applications, the noise photons from other nonlinear processes need to carefully addressed. We identify two potential noise sources for our system: Raman scattering and parametric fluorescence generation from spontaneous four wave mixing. Both unwanted process, however, can be suppressed by selecting the wavelength of drive laser far-away from the coherently coupled telecom and visible modes. We envision the demonstrated strong coupling between two spectrally far-away optical modes renders such device a unique interface for connecting matter qubits at visible wavelength with flying qubits at telecom wavelength, enabling the distributed quantum computation network and quantum communications [23, 35].

We thank Liang Jiang for stimulating discussion and Michael Power and Dr. Michael Rooks for assistance in device fabrication. H.X.T. acknowledges support from DARPA and a Packard Fellowship in Science and Engineering.

[1] R. J. Thompson, G. Rempe, and H. J. Kimble, Phys. Rev. Lett. 68, 1132 (1992).
[2] E. Peter, P. Senellart, D. Martrou, A. Lemaitre, J. Hours, J. M. Gerard, and J. Bloch, Phys. Rev. Lett. 95, 067401 (2005).
[3] J. Huang and P. Kumar, Phys. Rev. Lett. 68, 2153 (1992).
[4] M. T. Rakher, L. Ma, O. Slattery, X. Tang, and K. Srinivasan, Nature Photon. 4, 786 (2010).
[5] K. De Greve et al., Nature 491, 421 (2012).
[6] D. V. Strekalov, A. S. Kowligy, Y.-P. Huang, and P. Kumar, New J. Phys. 16, 053025 (2014).
[7] M. A. Foster, A. C. Turner, J. E. Sharping, B. S. Schmidt, M. Lipson, and A. L. Gaeta, Nature 441, 960 (2006).
[8] A. H. Gnauck, R. M. Jopson, C. J. McKinstrie, J. C. Centanni, and S. Radic, Opt. Express 14, 8989 (2006).
[9] I. Agha, M. Davanço, B. Thurston, and K. Srinivasan, Opt. Lett. 37, 2997 (2012).
[10] C. Dong, V. Fiore, M. C. Kuzyk, and H. Wang, Science 338, 1609 (2012).
[11] J. T. Hill, A. H. Safavi-Naeini, J. Chan, and O. Painter, Nature Commun. 3, 1196 (2012).
[12] D. J. Moss, R. Morandotti, A. L. Gaeta, and M. Lipson, Nature Photon. 7, 597 (2013).
[13] B. J. M. Hausmann, I. Bulu, V. Venkataraman, P. Deotare, and M. Lončar, Nature Photon. 8, 369 (2014).
[14] D. F. Welch et al., IEEE J. Sel. Top. Quantum Electron. 13, 22 (2007).
[15] A. Khilo et al., Opt. Express 20, 4454 (2012).
[16] C. Xiong, W. H. P. Pernice, X. Sun, C. Schuck, K. Y. Fong, and H. X. Tang, New J. Phys. 14, 95014 (2012).
[17] J. M. Dobrindt, I. Wilson-Rae, and T. J. Kippenberg, Phys. Rev. Lett. 101, 263602 (2008).
[18] J. Kim, M. C. Kuzyk, K. Han, H. Wang, and G. Bahl, Nature Phys. 11, 275 (2015).
[19] C.-H. Dong, Z. Shen, C.-L. Zou, Y.-L. Zhang, W. Fu, and G.-C. Guo, Nature Commun. 6, 6193 (2015).
[20] D. Jalas et al., Nature Photon. 7, 579 (2013).
[21] L. D. Tzuang, K. Fang, P. Nussenzveig, S. Fan, and M. Lipson, Nature Photon. 8, 701 (2014).
[22] B. Peng, Ş. K. Özdemir, F. Lei, F. Monifi, M. Gianfreda, G. L. Long, S. Fan, F. Nori, C. M. Bender, and L. Yang, Nature Phys. 10, 394 (2014).
[23] H. J. Kimble, Nature 453, 1023 (2008).
[24] C. Xiong, W. Pernice, K. K. Ryu, C. Schuck, K. Y. Fong, T. Palacios, and H. X. Tang, Opt. Express 19, 10462 (2011).
[25] J. S. Levy, M. A. Foster, A. L. Gaeta, and M. Lipson, Opt. Express 19, 11415 (2011).
[26] See Supplemental Material [url], which includes Refs. [27-29].
[27] L. Fan, J. Wang, L. T. Varghese, H. Shen, B. Niu, Y. Xuan, A. M. Weiner, and M. Qi, Science 335, 447 (2012).
[28] Y. Shi, Z. Yu, and S. Fan, Nature Photon. 9, 388 (2015).
[29] D. F. Walls & G. J. Milburn, Quantum optics. (Springer, 2007).
[30] M. Cai, O. Painter, and K. J. Vahala, Phys. Rev. Lett. 85, 74 (2000).
[31] S. Weis, R. Rivière, S. Deléglise, E. Gavartin, O. Arcizet, A. Schliesser, and T. J. Kippenberg, Science 330, 1520 (2010).
[32] S. Gröblacher, K. Hammerer, M. R. Vanner, and M. Aspelmeyer, Nature 460, 724 (2009).
[33] X. Zhang, N. Zhu, C.-L. Zou, and H. X. Tang, arXiv 1510.03545 (2015).
[34] W. H. P. Pernice, C. Xiong, C. Schuck, and H. X. Tang, Appl. Phys. Lett. 100, 223501 (2012).
[35] M. G. Raymer and K. Srinivasan, Phys. Today 65, 32 (2012).